Acidic nuclear phosphoprotein 32kDa (ANP32)B-deficient mouse reveals a hierarchy of ANP32 importance in mammalian development

Patrick T. Reilly[a], Samia Afzal[b,c], Chiara Gorrini[b], Koren Lui[b], Yury V. Bukhman[b,1], Andrew Wakeham[b], Jillian Haight[b], Teo Wei Ling[a], Carol C. Cheung[b], Andrew J. Elia[b], Patricia V. Turner[d], and Tak Wah Mak[a,b,2]

[a]Division of Cellular and Molecular Research, National Cancer Centre Singapore, Singapore 169610; [b]Campbell Family Cancer Research Institute, University Health Network, Toronto, ON, Canada M5G 2C1; [c]Graduate Program in Immunology, University of Toronto, Toronto, ON, Canada M5S 1A8; and [d]Department of Pathobiology, Ontario Veterinary College, University of Guelph, Guelph, ON, Canada N1G 2W1

Contributed by Tak Wah Mak, April 20, 2011 (sent for review February 18, 2011)

The highly conserved ANP32 proteins are proposed to function in a broad array of physiological activities through molecular mechanisms as diverse as phosphatase inhibition, chromatin regulation, caspase activation, and intracellular transport. On the basis of previous analyses of mice bearing targeted mutations of *Anp32a* or *Anp32e*, there has been speculation that all ANP32 proteins play redundant roles and are dispensable for normal development. However, more recent work has suggested that ANP32B may in fact have functions that are not shared by other ANP32 family members. Here we report that *ANP32B* expression is associated with a poor prognosis in human breast cancer, consistent with the increased levels of *Anp32b* mRNA present in proliferating wild-type (WT) murine embryonic fibroblasts and stimulated WT B and T lymphocytes. Moreover, we show that, contrary to previous assumptions, *Anp32b* is very important for murine embryogenesis. In a mixed genetic background, ANP32B-deficient mice displayed a partially penetrant perinatal lethality that became fully penetrant in a pure C57BL/6 background. Surviving ANP32B-deficient mice showed reduced viability due to variable defects in various organ systems. Study of compound mutants lacking ANP32A, ANP32B, and/or ANP32E revealed previously hidden roles for ANP32A in mouse development that became apparent only in the complete absence of ANP32B. Our data demonstrate a hierarchy of importance for the mammalian *Anp32* genes, with *Anp32b* being the most critical for normal development.

cell growth | mouse embryogenesis | premature aging

ANP32B (a.k.a. APRIL, PAL31, PHAP1b) is a mammalian member of the highly conserved acidic nuclear phosphoprotein 32kDa (ANP32) family of gene products (1). These metazoan-specific factors are characterized by the presence of an amino-terminal leucine-rich repeat domain and a carboxyl-terminal region that is highly enriched in acidic amino acid residues (2). These features are found in ANP32 proteins from mapmodulin, the single representative in *Drosophila*, and in the three vertebrate family members identified ANP32A, ANP32B, and ANP32E (1, 3).

The ANP32 proteins have been implicated in a broad array of physiological processes, including cell differentiation (4–7), apoptotic cell death (8–14), and cell proliferation (15–17). Diverse mechanisms have been postulated for how these proteins perform their function(s). Some studies indicate that ANP32 proteins may directly control enzymatic activities, such as via inhibition of protein phosphatase 2A (PP2A) (18–20) or activation of caspases (10, 11, 13, 14, 21). Other studies suggest that they may regulate intracellular transport at nuclear pores or microtubules (22–25). Several studies present evidence that nuclear ANP32 proteins may influence transcription either through the inhibitor of acetyl transferases complex (26–29) or by direct effects on transcription factors (30, 31). Most of the above reports have focused on ANP32A, the founding member of the ANP32 family, but none of these studies has specifically excluded a particular ANP32 protein as contributing to the activities examined.

More recent work has demonstrated functions that are exclusive to the ANP32B protein, at least in humans. First, ANP32B, but not ANP32A, controls the expression of the dendritic cell maturation factor CD83 by regulating the transport of its mRNA to the cytoplasm (22). Second, ANP32B modulates the activity of the transcription factor Kruppel-like factor 5 (KLF5), whereas ANP32A cannot (32). Finally, ANP32B is a caspase substrate, whereas ANP32A is not (33).

Reported loss-of-function mutants for ANP32 family members include two independently targeted ANP32A-deficient mice (34, 35), an ANP32E-deficient mouse (35), and a presumptive null mutant of *mapmodulin* in *Drosophila* (36). All of these mutants were viable and fertile with no obvious abnormalities. Here, we report on the phenotype of *Anp32b*-deficient ($Anp32b^{-/-}$) mice and, using compound mutants, show that ANP32 family members are not completely redundant in mammals. We demonstrate that ANP32B is the most important ANP32 family member for mammalian development and likely plays a complex role in sustaining viability that has yet to be completely defined. In addition, we provide evidence that the level of *ANP32B* mRNA expression in human breast cancers may serve as a prognostic marker.

Results

ANP32B as a Potential Prognostic Marker in Human Cancer. Reports that *ANP32B* expression was related to cell proliferation (15, 17) prompted us to investigate whether *ANP32B* expression was altered in human tumor samples. We examined the relationship between *ANP32B* mRNA expression and breast cancer patient prognosis using information from three available studies, namely the NEJM (*New England Medical Journal*) (37), the BMC (*BMC Genomics*) (38), and the PNAS datasets (39). When we compared the survival of these three groups of patients among all three datasets, we found that patients whose tumors showed the highest *ANP32B* mRNA levels had significantly shorter survival times using the Cox proportional hazard model ($P < 10^{-4}$). To display this effect, we stratified the patients in these datasets into three major groups: those with tumors expressing high levels of *ANP32B* mRNA (highest 33.3% or tertile), those with tumors with medium *ANP32B* mRNA levels (middle tertile), and those with tumors with low *ANP32B* mRNA levels (lowest tertile).

Author contributions: P.T.R. and T.W.M. designed research; P.T.R., S.A., C.G., K.L., A.W., J.H., T.W.L., C.C.C., and A.J.E. performed research; P.T.R., S.A., C.G., Y.V.B., P.V.T., and T.W.M. analyzed data; and P.T.R. and T.W.M. wrote the paper.

The authors declare no conflict of interest.

Freely available online through the PNAS open access option.

[1]Present address: Great Lakes Bioenergy Research Center, University of Wisconsin, Madison, WI 53706.

[2]To whom correspondence should be addressed. E-mail: tmak@uhnres.utoronto.ca.

This article contains supporting information online at www.pnas.org/lookup/suppl/doi:10.1073/pnas.1106211108/-/DCSupplemental.

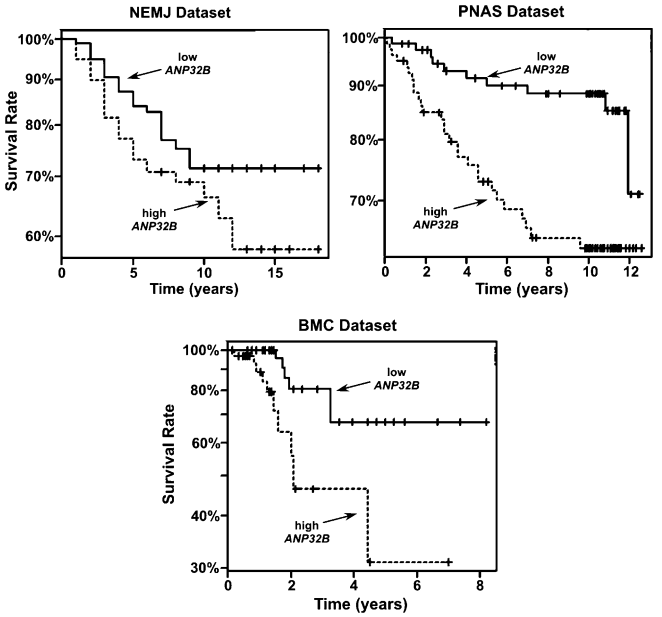

Fig. 1. *ANP32B* mRNA expression is a marker for aggressive breast cancer. Survival analyses of patients with tumors expressing the highest levels of *ANP32B* mRNA (highest tertile: dashed line), and patients with tumors expressing the lowest levels of *ANP32B* mRNA (lowest tertile: solid line). The middle tertile is not shown. Values were acquired from three separate datasets: NEMJ (37), PNAS (39), and BMC (38).

Here, the survival effect of the highest and lowest *ANP32B*-expressing tumors is clearly demonstrated (Fig. 1; middle tertile not shown). These results imply that elevated ANP32B expression in a tumor may be a marker of poor patient prognosis.

***Anp32b* mRNA Levels Are Linked to Cell Proliferation in Mice.** The less favorable prognosis of breast cancer patients with high *ANP32B*-expressing tumors suggested that the elevated *ANP32B* in these samples might be linked to more aggressive tumor cell proliferation. To investigate this hypothesis, we performed Northern blot analysis of a wide range of tissues from adult wild-type (WT) mice. We found that *Anp32b* expression was low (relative to *Gapdh*) in tissues where less cell proliferation usually occurs, i.e., in brain tissue (Fig. 2*A*). In contrast, tissues that generally have high cell proliferation rates, i.e., spleen and thymus, showed higher relative levels of *Anp32b* mRNA expression. We confirmed this pattern at the mRNA level by quantitating *Anp32b* expression (relative to *Tbp*) using quantitative RT-PCR (Fig. S1*A*). Again, proliferative tissues such as the spleen and thymus showed elevated levels of *Anp32b* mRNA, whereas the forebrain and hindbrain exhibited only low *Anp32b* expression. These data further suggest a link between *Anp32b* level and rate of cell proliferation.

To test whether proliferative stimuli could induce *Anp32b* expression, we subjected WT primary mouse embryo fibroblasts (MEFs) to serum deprivation to induce cell cycle arrest and then stimulated their proliferation by restoring standard serum levels to the culture. Under conditions of serum deprivation, *Anp32b* mRNA was barely detectable in WT MEFs (Fig. 2*B*). However, upon the addition of serum and the resumption of proliferation, *Anp32b* mRNA was significantly increased ($P < 0.01$) by more than 38-fold relative to control *Actb*. Under identical conditions, the induction of mRNA encoding *Myc*, a well-documented early proliferation marker, achieved a 4.8-fold increase (Fig. S1*B*). Similarly, WT B cells stimulated with LPS, and WT T cells activated with anti-CD3 plus anti-CD28 antibodies (activators of the T-cell receptor complex and T-cell costimulatory complex, respectively), showed significant elevation ($P < 0.01$) of *Anp32b* mRNA levels (Fig. 2*C*). These results indicate that *Anp32b* is up-regulated under conditions that favor cell proliferation.

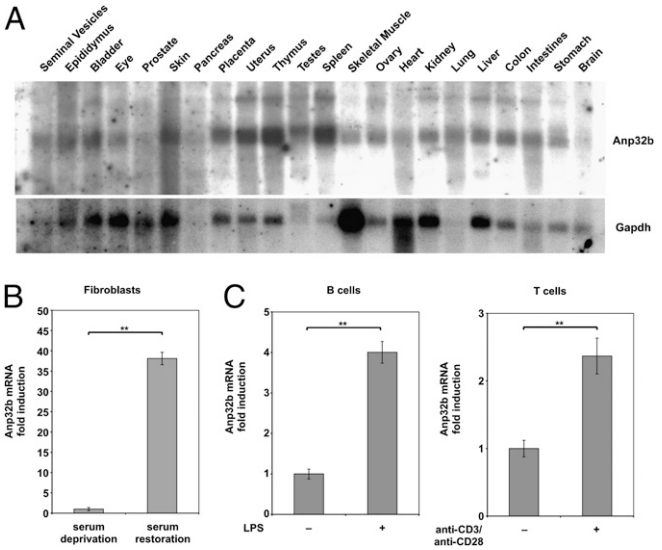

Fig. 2. Elevated *Anp32b* mRNA expression correlates with increased cell proliferation. (*A*) Correlation with highly proliferative tissues. A commercial mouse tissue blot was examined by Northern blotting to detect *Anp32b* mRNA. *Gapdh*: relative expression control. *Anp32b* mRNA is decreased relative to *Gapdh* in brain and muscle. (*B*) Correlation with nutrient-induced proliferation. WT MEFs were deprived of serum for 72 h and then resupplied with medium containing 10% FBS for 24 h. *Anp32b* mRNA levels were determined by qPCR relative to β-actin. Data shown are the mean ± SD of two independent WT MEF cultures. $^{**}P < 0.01$. (*C*) Correlation with lymphocyte stimulation. (*Left*) Purified B cells from WT mice were treated with 1 μg/mL LPS for 24 h. (*Right*) Purified T cells from WT mice were stimulated with plate-bound anti-CD3 (2 μg/mL) plus anti-CD28 (0.2 μg/mL) for 36 h. In both cases, *Anp32b* mRNA levels were determined by qPCR relative to 18S rRNA. Results shown are the mean ± SD of triplicates and are expressed as fold increase over levels in untreated controls. Results are representative of two trials. $^{**}P < 0.01$.

Gene Targeting of *Anp32b* in Mice. To investigate the physiological functions of ANP32B in vivo, we generated mice in which the *Anp32b* gene was disrupted by replacing the genomic region containing exons 2, 3, and 4 with a pgk-neo expression cassette (Fig. 3*A*). This mutation results in an mRNA in which the last 17 codons of exon 1 are linked to an out-of-frame exon 5. Southern blotting of the genomic DNA of E14K ES cell clones demonstrated a single appropriate insertion of the pgk-neo sequence (Fig. 3*B*, *Left*). $Anp32b^{+/-}$ mice (mixed 129:C57BL/6 background) were then generated and intercrossed to create $Anp32b^{-/-}$ progeny. Genomic deletion was confirmed in primary MEFs derived from $Anp32b^{-/-}$ embryos using a flanking genomic probe (Fig. 3*B*, *Right*). Immunoblotting of extracts of $Anp32b^{-/-}$ MEFs demonstrated that there was no detectable Anp32b protein in nullizygous mutants (Fig. 3*C*).

ANP32B Protects Against Perinatal Lethality. The intercrossing of our mixed-bred 129:C57BL/6 $Anp32b^{+/-}$ mice to generate $Anp32b^{-/-}$ mutants revealed a defect in mutant mouse viability. At the time of weaning (~21 d of age), $Anp32b^{-/-}$ mice were present at a far lower frequency (7%) than the 25% expected according to the standard Mendelian distribution ($P < 0.01$; Table 1). To exclude the possibility that the observed defect was due to a linked mutation present in the ES cell clones, we backcrossed the *Anp32b* mutant allele into the C57BL/6 background for six generations. The penetrance of the survival defect was increased in the pure C57BL/6 background ($P < 0.01$; Table 2), strongly suggesting that the defect in viability is not attributable to a linked gene mutation.

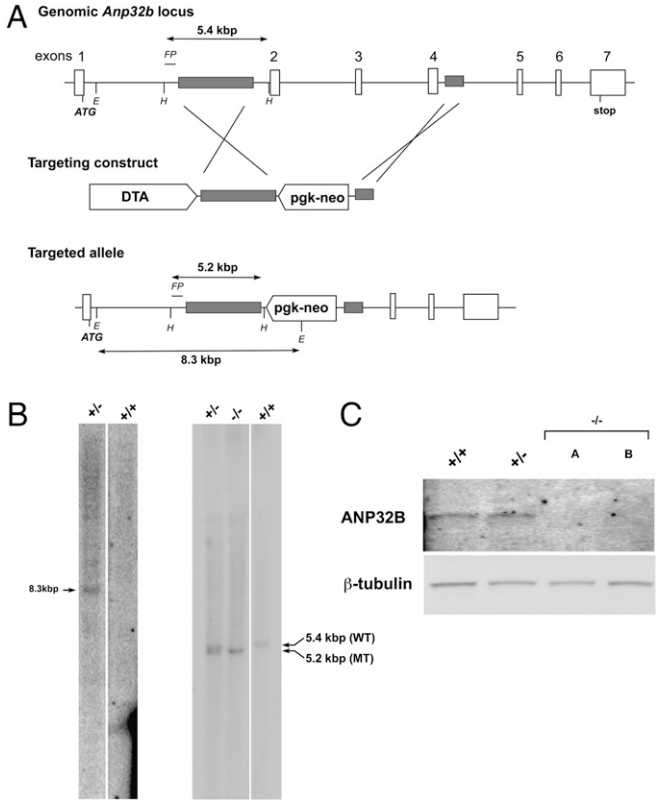

Fig. 3. Generation and validation of ANP32B-deficient mice. (*A*) Targeting of the murine *Anp32b* gene. (*Top*) Murine genomic *Anp32b* locus showing exons and regions of homology (gray). *FP*: flanking probe detecting intron 1. *H:* HindIII; *E:* EagI sites. The translation start site (ATG) and stop sites are shown. (*Middle*) Targeting construct that replaced exons 2–4 with a pgk-neo cassette. DTA: diphtheria toxin A sequence for negative selection. (*Bottom*) Targeted *Anp32b* allele. Diagnostic HindIII fragments for the WT *Anp32b* allele (5.4 kb) and the targeted *Anp32b* allele (5.2 kb), as well as the diagnostic EagI fragment for neo insertion (8.3 kb) are shown. (*B*) Confirmation of *Anp32b* gene deletion. (*Left*) DNA from $Anp32b^{+/-}$ and $Anp32b^{+/+}$ ES cells was Southern-blotted with a neo probe to confirm a single vector insertion. (*Right*) DNA from MEFs derived from $Anp32b^{+/-}$, $Anp32b^{-/-}$, or $Anp32b^{+/+}$ mice was Southern-blotted using the flanking probe. WT HindIII band = 5.4 kb; mutant (MT) HindIII band = 5.2 kb. (*C*) Loss of ANP32B protein. $Anp32b^{+/+}$, $Anp32b^{+/-}$ and $Anp32b^{-/-}$ MEFs were immunoblotted to detect ANP32B protein. A and B are MEFs from two different $Anp32b^{-/-}$ littermate embryos. β-Tubulin: loading control. Results shown in *B* and *C* are representative of three trials.

To define precisely when the majority of $Anp32b^{-/-}$ mice died, we monitored litters from the time of first detection (12 h postnatal) until weaning. However, virtually all $Anp32b^{-/-}$ mice that were evident at first detection survived to adulthood. This observation indicated that the developmental problem(s) killing most $Anp32b^{-/-}$ mice occurred either during embryogenesis or before normal litter detection. In the course of generating our primary MEFs, we noted that $Anp32b^{-/-}$ embryos were present at approximately Mendelian rates on embryonic day 14.5 (E14.5). We therefore chose to follow the fate of $Anp32b^{-/-}$ embryos from late embryogenesis until early time points after birth. Among litters examined immediately after birth, some $Anp32b^{-/-}$ pups never initiated breathing, whereas others were able to nurse, at least initially. Timed pregnancy studies revealed that E17.5 $Anp32b^{-/-}$ embryos were present at approximately Mendelian frequency (Table 3). No defect detectable by gross inspection was evident in any E17.5 $Anp32b^{-/-}$ embryos of the mixed background (Fig. 4 *A* and *B*). Examination of $Anp32b^{-/-}$ embryos of the pure C57BL/6 background showed that these animals also

Table 1. Reduced survival rate of *Anp32b*-deficient mice

	$Anp32b^{+/+}$	$Anp32b^{+/-}$	$Anp32b^{-/-}$
Expected	39	78	39
Observed*	57	87	11

$Anp32b^{+/-}$ mice of mixed 129ola:C57BL/6 background were intercrossed and pups were genotyped at time of weaning (between postnatal 19 and 22 d). "Expected" indicates the distribution for the indicated total number of mice under conditions of normal Mendelian segregation. "Observed" indicates the actual numbers of mice of the indicated genotypes obtained. *$P < 0.01$ by χ^2 analysis.

remained viable until at least E17.5. Taken together, our data suggest that the defect(s) killing $Anp32b^{-/-}$ mice occur perinatally, i.e., at or very near the time of birth.

Rigorous pathological examinations of eight $Anp32b^{-/-}$ E17.5 embryos as well as three postnatal day 1 (P1) pups of both the mixed 129:C57BL/6 and the pure C57BL/6 backgrounds revealed no obvious gross abnormalities in a majority of embryos examined. Some $Anp32b^{-/-}$ E17.5 embryos did show subtle and sporadic craniofacial abnormalities, including overlarge ventricles in the brain, expanded inner ear cavities, and palate closure defects. The heart and lungs were not obviously affected. Interestingly, large hematomas in the liver, aortic arch, or umbilical artery were observed in three of eight E17.5 embryos and in one of three P1 pups of the mixed mutant background. However, no one defect appeared to be responsible for the perinatal lethality of all $Anp32b^{-/-}$ mice.

Surviving $Anp32b^{-/-}$ Mice Show Reduced Size and Decreased Life Span. To investigate the effects of ANP32B deficiency in adult mice, we monitored our surviving mixed-bred $Anp32b^{-/-}$ mice and their littermates from time of weaning until age approximately 1 y. At time of weaning, surviving $Anp32b^{-/-}$ female mice weighed, on average, 42% less than WT females and 35% less than their female $Anp32b^{+/-}$ littermates ($P < 0.05$; Fig. 4*C*). A similar trend was seen for males, although the differences did not reach statistical significance in this analysis (Fig. S2). When the data for male and female sex-matched littermates were combined, a statistically significant reduction in body weight was apparent when $Anp32b^{-/-}$ and $Anp32b^{+/-}$ littermates were compared ($P < 0.01$), as well as when $Anp32b^{-/-}$ and $Anp32b^{+/+}$ littermates were compared ($P < 0.05$).

Surviving $Anp32b^{-/-}$ mice were not robust and showed signs of premature aging. Many $Anp32b^{-/-}$ mutants exhibited early onset kyphosis in which the curvature of the upper spine was evident at 4 mo of age and severe by 6 mo (Fig. 4*D*). Increased hepatocyte polyploidy, another hallmark of premature aging, was also present in the aged $Anp32b^{-/-}$ mice. However, premature alopecia, which is a common aspect of early aging, was not seen in the kyphotic mice. Consistent with these phenotypic features, $Anp32b^{-/-}$ mice had a reduced life span ($P < 0.01$; Fig. 4*E*), but no consistent pathology could be identified as the cause of their premature death. Two cases of megacolon and two cases of hydroureter

Table 2. Genetic background influence survival rate of *Anp32b*-deficient mice

	$Anp32b^{+/+}$	$Anp32b^{+/-}$	$Anp32b^{-/-}$
Expected	36	72	36
Observed*	56	87	1

$Anp32b^{+/-}$ mice from congenic C57BL/6 background were intercrossed and pups were genotyped at time of weaning (between postnatal 19 and 22 d). "Expected" indicates the distribution for the indicated total number of mice under conditions of normal Mendelian segregation. "Observed" indicates the actual numbers of mice of the indicated genotypes obtained. *$P < 0.01$ by χ^2 analysis.

Table 3. Normal survival rate of *Anp32b*-deficient embryos at E17.5

	$Anp32b^{+/+}$	$Anp32b^{+/-}$	$Anp32b^{-/-}$
Expected	6	11	6
Observed*	8	8	6

$Anp32b^{+/-}$ mice were intercrossed and embryos were genotyped at time E17.5. "Expected" indicates the distribution for the indicated total number of embryos under conditions of normal Mendelian segregation. "Observed" indicates the actual numbers of embryos of the indicated genotypes obtained. *No significant differences were found.

causing severe morbidity were observed, but the other five aged $Anp32b^{-/-}$ mice died without identifiable cause.

Normal Cellular Apoptosis and Proliferation in the Absence of ANP32B. We next turned to in vitro studies in an attempt to identify the cause of the viability defects in $Anp32b^{-/-}$ mice. Because *Anp32b* has been implicated in the regulation of caspase activity (10, 33), we first investigated the response of $Anp32b^{-/-}$ thymocytes and transformed MEFs to a broad array of intrinsic and extrinsic apoptotic stimuli. However, no statistically significant differences between $Anp32b^{+/+}$ and $Anp32b^{-/-}$ cells of either type were observed (Fig. S3). Similarly, prompted by the conclusions of previous reports (15, 17), we investigated whether loss of ANP32B affected cell proliferation, but, again, no defects in in vitro proliferation were found for $Anp32b^{-/-}$ primary MEFs, thymocytes, or splenocytes (Fig. S4).

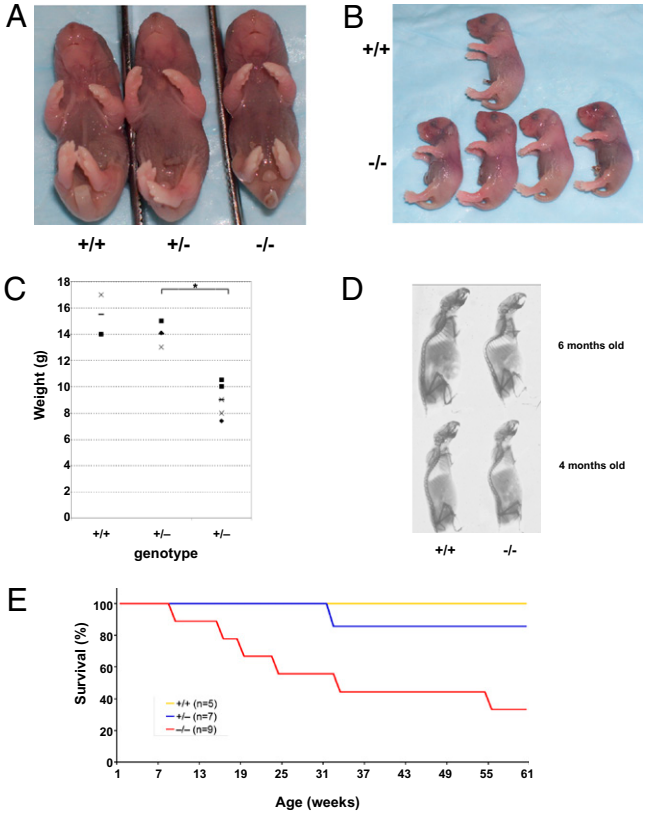

Fig. 4. Phenotypes of ANP32B-deficient mice. (*A* and *B*) Normal gross appearance. Embryos of the indicated *Anp32b* genotypes were collected at E17.5 and subjected to gross examination. (*A*) Rostral view. (*B*) Left side view. Tail fragments were removed for genotyping purposes. No obvious abnormalities were seen. Embryos shown were derived from two different litters and are representative of a total of 10 examined per genotype. (*C*) Reduced body weight. $Anp32b^{-/-}$ mice were weighed alongside their $Anp32b^{+/+}$ or $Anp32b^{+/-}$ littermates at 3 wk of age. Results shown are values for individual mice. Horizontal bars are mean values. $*P < 0.05$. (*D*) Kyphosis. X-ray analysis was performed on littermate pairs of female $Anp32b^{+/+}$ and $Anp32b^{-/-}$ mice at 4 and 6 mo of age. Results shown are representative of over 10 mice examined per genotype per age. (*E*) Decreased life span. Survival curves of $Anp32b^{+/+}$, $Anp32b^{+/-}$ and $Anp32b^{-/-}$ littermates that lived past weaning age are shown. The reduced survival of $Anp32b^{-/-}$ mice is statistically significant, as determined by log-rank analysis ($P < 0.01$).

ANP32B Masks a Role for ANP32A in Essential Development. We have previously reported that neither the ANP32A-deficient nor the ANP32E-deficient mouse has any obvious abnormal phenotype (35). To determine whether deficiency for another Anp32 family member might expose the cause of the viability defect of our $Anp32b^{-/-}$ mice, we generated $Anp32b^{+/-};Anp32a^{+/-}$ and $Anp32b^{+/-};Anp32e^{+/-}$ double-mutant strains and intercrossed them. As shown in Table 4, heterozygosity for *Anp32a* further compromised development in the $Anp32b^{-/-}$ background ($P < 0.01$). Indeed, no $Anp32b^{-/-};Anp32a^{+/-}$ or $Anp32b^{-/-};Anp32a^{-/-}$ mouse survived to weaning. Thus, contrary to prevailing belief, ANP32A does have a subtle role in murine embryogenesis that is revealed only in the absence of ANP32B.

In contrast, loss of ANP32E did not further exacerbate the lethality associated with *Anp32b* deletion (Table 5). Although only one $Anp32b^{-/-};Anp32e^{-/-}$ mouse survived to weaning in this particular analysis, this rate was not statistically different from the survival rate expected for a mouse lacking only $Anp32b^{-/-}$ (Table 1). Furthermore, $Anp32b^{-/-};Anp32e^{+/-}$ mice exhibited a robust survival that stood in marked contrast to the fully penetrant lethality of $Anp32b^{-/-};Anp32a^{+/-}$ mice. When we attempted to generate triple mutants lacking ANP32A, ANP32B, and ANP32E, none were viable (as expected). Strikingly, a single functional *Anp32b* allele was sufficient to allow survival to weaning age in the mixed-bred background (Table S1), but a single functional *Anp32a* or *Anp32e* allele could not support mouse survival in the absence of ANP32B. These data indicate that there is a hierarchy of ANP32 protein functions in which ANP32B is the most important family member for embryogenesis, with ANP32A being of moderate importance and ANP32E being of least importance.

Discussion

In this study, we provide evidence that ANP32B may be a useful prognostic indicator in human breast cancer and describe the generation and characterization of the ANP32B-deficient mouse.

We carried out a meta-analysis of *ANP32B* mRNA levels in human breast cancers using three independent studies in which the patients were subject to different exclusion criteria and treatment regimens (37–39). Although ANP32B was not highlighted in the original individual analyses, our examination of the combined data indicates that elevated ANP32B expression correlates with shortened patient survival. We hypothesize that ANP32B does not control tumorigenesis itself but rather increases, or is a marker of, the robustness of the resulting tumor cells; that is, ANP32B is elevated in tumor cells exhibiting increased proliferation and thus aggression. Consistent with this hypothesis, we found that *Anp32b* mRNA was up-regulated in murine cells exhibiting enhanced proliferation in tissue culture and in vivo.

Our report identifies an ANP32 mutation with a strong adverse effect on development. We have shown that null mutation of *Anp32b* in mice results in highly penetrant perinatal lethality in a mixed genetic background and in fully penetrant lethality in a pure C57BL/6 background. The specific cause of this lethality remains unclear because surviving mixed-bred $Anp32b^{-/-}$ mice suffered from a range of pathologies. We speculate that, during the course of evolution, the ANP32 proteins, and particularly ANP32B, took on functions that were less dispensable for embryogenesis. The nature of these functions remains obscure, as our data indicate that loss of ANP32B does not consistently affect one organ and that the majority of these animals die just after E17.5, when most murine organogenesis is complete.

Table 4. Loss of *Anp32b* reveals a moderate viability defect attributable to *Anp32a*

	$Anp32b^{+/+}$			$Anp32b^{+/-}$			$Anp32b^{-/-}$		
	$Anp32a^{+/+}$	$Anp32a^{+/-}$	$Anp32a^{-/-}$	$Anp32a^{+/+}$	$Anp32a^{+/-}$	$Anp32a^{-/-}$	$Anp32a^{+/+}$	$Anp32a^{+/-}$	$Anp32a^{-/-}$
Mendelian	10	20	10	20	41	20	10	20	10
Expected	15	30	15	23	45	23	3	6	3
Observed*	15	25	20	28	43	23	8	0	0

Numbers of double-mutant mice of the indicated genotypes arising from the intercrossing of $Anp32a^{+/-}$;$Anp32b^{+/-}$ mice. "Mendelian" indicates the distribution for the indicated total number of mice under conditions of normal Mendelian segregation. "Expected" indicates the distribution for the Mendelian distributed numbers with integration of the observed rates of *Anp32b* lethality (Table 1). "Observed" indicates the actual numbers of mice of the noted genotypes obtained. Statistical probability is calculated against "Expected" ratios.
*$P < 0.01$ by χ^2 analysis.

Our histological examinations did not show any defects in vascular endothelium or smooth muscle, as might have been expected from previous reports on ANP32B functions (32, 40). However, our data regarding the incidence of hematomas in $Anp32b^{-/-}$ embryos do support a potential role for ANP32B in vascular development. Considering the recognized function of KLF5 in vasculogenesis (32), and the reported influence of ANP32B on KLF5-activated transcription, it is possible that the hematomas may have been due to defects in ANP32B-assisted, KLF5-activated transcription.

Our results confirm genetically that there is considerable functional overlap among ANP32 proteins. If different ANP32 proteins functioned in discrete cell types, or in different processes within the same cell, we would not have expected to see the synergistic effects that we observed in our compound mutants. However, our most dramatic finding is that mice carrying *Anp32b* mutations are sensitized to loss of *Anp32a*, a gene that has not previously been shown to have an effect on mouse development. These data establish that, contrary to previous assumptions, ANP32 family members are not all functionally redundant in vivo. Although mutations of multiple alleles of *Anp32a* or *Anp32e* are compatible with embryogenesis, at least one functional *Anp32b* allele must be present in any compound mutant for normal rates of survival. Thus, ANP32B is clearly the most important member of the ANP32 family, at least in mice.

The broad array of functions ascribed to various ANP32 family members in the literature suggests that certain reported biochemical functions may be artifactual. The data we have presented here, as well as in a previous publication (35), demonstrate that the *Anp32* genes are not likely to be broadly involved in apoptosis. Furthermore, no ANP32-deficient cells have yet shown proliferation defects, implying that ANP32-mediated inhibition of cell cycle control phosphatases, such as PP2A, may be redundant or have a limited impact on cell proliferation. Instead, we speculate that ANP32 proteins play a more direct role in controlling gene expression, likely through their reported activities in chromatin regulation and/or selective mRNA transport. In any case, regardless of the ANP32 protein function under investigation, our results indicate that future research aimed at understanding the shared functions of ANP32 proteins should concentrate on ANP32B.

Materials and Methods

Prognostic Marker Identification. Data were acquired from three publicly available datasets (37–39). The prognostic risk associated with particular gene expression was computed using application of the Cox proportional hazard regression model.

Northern Blotting. The multiple murine tissue blot for Northern analysis was acquired from Zyagen (catalog no. MN-MT-2). *Anp32b* mRNA was detected by hybridizing to a labeled probe consisting of the EcoRI–BamHI fragment at the 5′ end of the ORF. *Gapdh* was detected by probing with a 214-bp fragment that hybridized to exons 5, 6, and 7.

Real-Time RT-PCR. RNA was extracted from specified cell populations using a standard protocol and the RNeasy kit (Qiagen), quantified, and reverse-transcribed using a SuperScript II first-strand synthesis kit (Invitrogen). cDNA samples were then used as templates for quantitative real-time PCR (qPCR) using an ABI 7900HT detection system and SYBR Green (Applied Biosystems). Data were normalized to *Actb* (β-actin), *Tbp* mRNA, or *Rn18S* (18S rRNA). Primer sequences are provided in Table S2. Statistical significance of differences in normalized values were assessed by Student's *t* test.

Mice. Mice were maintained under specified-pathogen free conditions in individually ventilated cages and fed a 5% irradiated meal. $Anp32b^{-/-}$ mice analyzed in this study were derived from two separate homologous recombinant clones and analyzed in approximately equal proportion for all experiments. Unless otherwise stated, analyses were performed in the mixed-bred 129ola;C57BL/6 genetic background. Statistical analyses for weights and longevity were performed using Student's *t* test and log-rank analysis, respectively.

Plasmids and Primers. Sequences directing the expression of diphtheria toxin A in mouse ES cells were cloned into pBluescript (pgk-neo) to give the plasmid pBSneoDTA (35). Regions of the *Anp32b* gene adjacent to the targeted exons were cloned by high-fidelity PCR. Primers used to clone the upstream and downstream arms of homology into the XhoI site and XbaI site, respectively, are shown in Table S2.

Gene Targeting. Targeting constructs were linearized and transfected by electroporation into E14K mouse ES cells as previously described (41, 42). Southern probes used to detect *Anp32b* genomic sequences were amplified from genomic ES cell DNA. PCR primer sequences for *Anp32b* flanking probe generation are presented in Table S2.

Table 5. Loss of *Anp32b* does not reveal any defect attributable to *Anp32e*

	$Anp32b^{+/+}$			$Anp32b^{+/-}$			$Anp32b^{-/-}$		
	$Anp32e^{+/+}$	$Anp32e^{+/-}$	$Anp32e^{-/-}$	$Anp32e^{+/+}$	$Anp32e^{+/-}$	$Anp32e^{-/-}$	$Anp32e^{+/+}$	$Anp32e^{+/-}$	$Anp32e^{-/-}$
Mendelian	6	11	6	11	22	11	6	11	6
Expected	8	16	8	12	25	12	2	3	2
Observed	9	13	10	14	21	15	3	2	1

Number of double-mutant mice arising from the intercrossing of $Anp32e^{+/-}$;$Anp32b^{+/-}$ mice. "Mendelian" indicates the distribution for the indicated total number of mice under conditions of normal Mendelian segregation. "Expected" indicates the distribution for the Mendelian distributed numbers with integration of the observed rates of *Anp32b* lethality (Table 1). "Observed" indicates the actual numbers of mice of the noted genotypes obtained. No statistically significant deviation from "Expected" values was observed using χ^2 analysis.

Genotyping. For standard genotyping, PCR was performed on proteinase-treated biopsies. Primer sequences are provided in Table S2. Statistical analyses of progeny derived from intercrosses were performed using χ^2 analysis.

Immunoblotting. Mouse thymi were homogenized and lysed in buffer containing Nonidet P-40 detergent. Protein extracts (5 μg) were fractionated by SDS/PAGE, transferred to PVDF membranes, and probed with anti-ANP32B antibody (10843-1-AP; Proteintech) or anti–β-tubulin (loading control; Li-Cor Bioscience). Protein bands on blots were visualized using Li-Cor Odyssey standard protocols.

Cell Populations. Primary MEFs were prepared from littermate *Anp32b*$^{+/+}$, *Anp32b* $^{+/-}$, and *Anp32b* $^{-/-}$ E14.5 embryos derived from timed interbreedings of *Anp32b*$^{+/-}$ mice. For transformed MEFs, primary MEFs (5×10^5 cells) were infected with a retrovirus generated from pLPC E1A/ras$_{V12}$ using published techniques (43). Single-cell suspensions of total thymocytes were prepared from three sex-matched littermate pairs of *Anp32b* $^{+/+}$ and *Anp32b* $^{-/-}$ mice (4–8 wk old). Single-cell suspensions derived from spleen or lymph nodes were treated with red blood cell lysis buffer (Sigma) to remove erythrocytes, and B and T cells were purified using the IMag cell separation system (Becton Dickinson). Briefly, total leukocytes were incubated with mouse anti-CD16/32 blocking antibodies, after which T cells were negatively selected using biotinylated anti-Ter119/B220/CD19/CD11b/Nk1.1/CD11c antibodies, and B cells were positively selected using biotinylated anti-CD19/B220 antibodies.

Apoptosis. Apoptosis assays were performed as described previously (35, 44). Briefly, cells were exposed to apoptotic stimuli as detailed in Fig. S3 and cultured overnight in medium containing penicillin/streptomycin, 10% FBS, and L-glutamine. Viability was determined by propidium iodide exclusion and flow cytometry using a FACScaliber (BD Pharmingen).

Proliferation. The growth of primary MEFs in culture was analyzed as previously described (35). Purified B cells were treated with 1 μg/mL LPS for 24 h. Purified T cells were stimulated by seeding on plates precoated with anti-CD3 and anti-CD28 antibodies as previously described (45). Statistical differences in cell growth were assessed using Student's *t* test.

ACKNOWLEDGMENTS. We thank Arda Shahinian, Gordon Duncan, Jennifer Silvester, Jaselyn Becz-Ortiz, Low Mei Jun, and Melissa Madden for technical assistance and Mary Saunders for scientific editing of the manuscript. This research was partially supported by the Prostate Cancer Research Foundation of Canada, the Department of Defense (Grant PC020806), and the Singapore Millennium Foundation.

1. Santa-Coloma TA (2003) Anp32e (Cpd1) and related protein phosphatase 2 inhibitors. *Cerebellum* 2:310–320.
2. Huyton T, Wolberger C (2007) The crystal structure of the tumor suppressor protein pp32 (Anp32a): Structural insights into Anp32 family of proteins. *Protein Sci* 16: 1308–1315.
3. Matilla A, Radrizzani M (2005) The Anp32 family of proteins containing leucine-rich repeats. *Cerebellum* 4:7–18.
4. Anisimov SV, et al. (2002) SAGE identification of gene transcripts with profiles unique to pluripotent mouse R1 embryonic stem cells. *Genomics* 79:169–176.
5. Brody JR, et al. (2004) pp32 reduction induces differentiation of TSU-Pr1 cells. *Am J Pathol* 164:273–283.
6. Kular RK, Cvetanovic M, Siferd S, Kini AR, Opal P (2009) Neuronal differentiation is regulated by leucine-rich acidic nuclear protein (LANP), a member of the inhibitor of histone acetyltransferase complex. *J Biol Chem* 284:7783–7792.
7. Puente LG, Carrière JF, Kelly JF, Megeney LA (2004) Comparative analysis of phosphoprotein-enriched myocyte proteomes reveals widespread alterations during differentiation. *FEBS Lett* 574:138–144.
8. Adegbola O, Pasternack GR (2005) Phosphorylated retinoblastoma protein complexes with pp32 and inhibits pp32-mediated apoptosis. *J Biol Chem* 280: 15497–15502.
9. Hoffarth S, et al. (2008) pp32/PHAPI determines the apoptosis response of non-small-cell lung cancer. *Cell Death Differ* 15:161–170.
10. Jiang X, et al. (2003) Distinctive roles of PHAP proteins and prothymosin-alpha in a death regulatory pathway. *Science* 299:223–226.
11. Mazroui R, et al. (2008) Caspase-mediated cleavage of HuR in the cytoplasm contributes to pp32/PHAP-I regulation of apoptosis. *J Cell Biol* 180:113–127.
12. Pan W, et al. (2009) PHAPI/pp32 suppresses tumorigenesis by stimulating apoptosis. *J Biol Chem* 284:6946–6954.
13. Schafer ZT, et al. (2006) Enhanced sensitivity to cytochrome c-induced apoptosis mediated by PHAPI in breast cancer cells. *Cancer Res* 66:2210–2218.
14. Sun W, et al. (2006) Proliferation related acidic leucine-rich protein PAL31 functions as a caspase-3 inhibitor. *Biochem Biophys Res Commun* 342:817–823.
15. Amasaki H, et al. (2003) Distributional changes of BrdU, PCNA, E2F1 and PAL31 molecules in developing murine palatal rugae. *Ann Anat* 185:517–523.
16. Fukukawa C, Tanuma N, Okada T, Kikuchi K, Shima H (2005) pp32/I-1(PP2A) negatively regulates the Raf-1/MEK/ERK pathway. *Cancer Lett* 226:155–160.
17. Sun W, et al. (2001) PAL31, a nuclear protein required for progression to the S phase. *Biochem Biophys Res Commun* 280:1048–1054.
18. Costanzo RV, et al. (2006) Anp32e/Cpd1 regulates protein phosphatase 2A activity at synapses during synaptogenesis. *Eur J Neurosci* 23:309–324.
19. Li M, Makkinje A, Damuni Z (1996) Molecular identification of I1PP2A, a novel potent heat-stable inhibitor protein of protein phosphatase 2A. *Biochemistry* 35:6998–7002.
20. Radrizzani M, et al. (2001) Differential expression of CPD1 during postnatal development in the mouse cerebellum. *Brain Res* 907:162–174.
21. Hill MM, Adrain C, Duriez PJ, Creagh EM, Martin SJ (2004) Analysis of the composition, assembly kinetics and activity of native Apaf-1 apoptosomes. *EMBO J* 23: 2134–2145.
22. Fries B, et al. (2007) Analysis of nucleocytoplasmic trafficking of the HuR ligand APRIL and its influence on CD83 expression. *J Biol Chem* 282:4504–4515.
23. Gallouzi IE, Brennan CM, Steitz JA (2001) Protein ligands mediate the CRM1-dependent export of HuR in response to heat shock. *RNA* 7:1348–1361, and partial retraction (2003) 9:1410.
24. Itin C, Ulitzur N, Mühlbauer B, Pfeffer SR (1999) Mapmodulin, cytoplasmic dynein, and microtubules enhance the transport of mannose 6-phosphate receptors from endosomes to the trans-golgi network. *Mol Biol Cell* 10:2191–2197.
25. Opal P, et al. (2003) Mapmodulin/leucine-rich acidic nuclear protein binds the light chain of microtubule-associated protein 1B and modulates neuritogenesis. *J Biol Chem* 278:34691–34699.
26. Kutney SN, Hong R, Macfarlan T, Chakravarti D (2004) A signaling role of histone-binding proteins and INHAT subunits pp32 and Set/TAF-Ibeta in integrating chromatin hypoacetylation and transcriptional repression. *J Biol Chem* 279:30850–30855.
27. Schneider R, Bannister AJ, Weise C, Kouzarides T (2004) Direct binding of INHAT to H3 tails disrupted by modifications. *J Biol Chem* 279:23859–23862.
28. Seo SB, et al. (2002) Regulation of histone acetylation and transcription by nuclear protein pp32, a subunit of the INHAT complex. *J Biol Chem* 277:14005–14010.
29. Tochio N, et al. (2010) Solution structure of histone chaperone ANP32B: Interaction with core histones H3-H4 through its acidic concave domain. *J Mol Biol* 401:97–114.
30. Cvetanovic M, et al. (2007) The role of LANP and ataxin 1 in E4F-mediated transcriptional repression. *EMBO Rep* 8:671–677.
31. Loven MA, et al. (2004) A novel estrogen receptor alpha-associated protein alters receptor-deoxyribonucleic acid interactions and represses receptor-mediated transcription. *Mol Endocrinol* 18:2649–2659.
32. Munemasa Y, et al. (2008) Promoter region-specific histone incorporation by the novel histone chaperone ANP32B and DNA-binding factor KLF5. *Mol Cell Biol* 28: 1171–1181.
33. Shen SM, et al. (2010) Downregulation of ANP32B, a novel substrate of caspase-3, enhances caspase-3 activation and apoptosis induction in myeloid leukemic cells. *Carcinogenesis* 31:419–426.
34. Opal P, et al. (2004) Generation and characterization of LANP/pp32 null mice. *Mol Cell Biol* 24:3140–3149.
35. Reilly PT, et al. (2010) Generation and characterization of the Anp32e-deficient mouse. *PLoS ONE* 5:e13597.
36. Buszczak M, et al. (2007) The carnegie protein trap library: A versatile tool for Drosophila developmental studies. *Genetics* 175:1505–1531.
37. van de Vijver MJ, et al. (2002) A gene-expression signature as a predictor of survival in breast cancer. *N Engl J Med* 347:1999–2009.
38. Hu Z, et al. (2006) The molecular portraits of breast tumors are conserved across microarray platforms. *BMC Genomics* 7:96.
39. Miller LD, et al. (2005) An expression signature for p53 status in human breast cancer predicts mutation status, transcriptional effects, and patient survival. *Proc Natl Acad Sci USA* 102:13550–13555.
40. Zippo A, De Robertis A, Bardelli M, Galvagni F, Oliviero S (2004) Identification of Flk-1 target genes in vasculogenesis: Pim-1 is required for endothelial and mural cell differentiation in vitro. *Blood* 103:4536–4544.
41. Okada H, et al. (2002) Generation and characterization of Smac/DIABLO-deficient mice. *Mol Cell Biol* 22:3509–3517.
42. Ruland J, et al. (2001) p53 accumulation, defective cell proliferation, and early embryonic lethality in mice lacking tsg101. *Proc Natl Acad Sci USA* 98:1859–1864.
43. Lin AW, et al. (1998) Premature senescence involving p53 and p16 is activated in response to constitutive MEK/MAPK mitogenic signaling. *Genes Dev* 12:3008–3019.
44. Zaugg K, et al. (2007) Cross-talk between Chk1 and Chk2 in double-mutant thymocytes. *Proc Natl Acad Sci USA* 104:3805–3810, and correction (2007) 104: 8196.
45. Dufner A, et al. (2008) CARD6 is interferon inducible but not involved in nucleotide-binding oligomerization domain protein signaling leading to NF-kappaB activation. *Mol Cell Biol* 28:1541–1552.